JOURNAL OF SOLID STATE CHEMISTRY 84, 314–334 (1990)

Continuous Series of One-Dimensional Structures in Compounds Based on M_2X_3 (M = Sb, Bi; X = Se, Te)

N. FRANGIS,*† S. KUYPERS,† C. MANOLIKAS,* G. VAN TENDELOO,† J. VAN LANDUYT,† AND S. AMELINCKX†

Solid State Physics Section, Aristotle University of Thessaloniki, GR-54006 Thessaloniki, Greece; and †University of Antwerp (RUCA), Groenenborgerlaan 171, B-2020 Antwerpen, Belgium

Received May 17, 1989; in revised form October 6, 1989

For compounds of the type M_2X_3 (Bi_2Te_3, Bi_2Se_3, Sb_2Te_3), doping with Ge (Sn or Pb), as well as addition of excess cations, leads to the formation of continuous series of 1 D superstructures which can now be characterized by means of electron microscopy. The systems $Ge_\delta Bi_2Te_3$ and $Bi_{2+\delta}Se_3$ are discussed as model systems. Analysis of the electron diffraction patterns with the fractional shift method suggests the superstructures are built up of sequences of five- and seven-layer lamellae. This interpretation is confirmed by direct (high resolution) images. From a comparison between experimental high resolution images and computed images, a model for the five- and seven-layer lamellae is presented. A modified "cut and projection" method is described and applied to derive the sequences of "5" and "7" bands from the (approximate) q-values of the (quasi)commensurate diffraction patterns. © 1990 Academic Press, Inc.

1. Introduction

The compounds of the type $M_{2+\delta}X_3$ with M = Sb, Bi and X = Te, Se have been the subject of intense study, especially since it was found that the diffraction patterns and therefore the crystal structures seem to change rapidly and nonsystematically with the metal excess δ, very long period superstructures being formed (*1*). Also the effect of the substitution of Bi and Sb by other metal atoms such as Ge, Pb, Sn . . . on the structures has been studied because these doped compounds are of interest for thermoelectric applications. In particular structures were proposed for compounds such as $PbBi_4Te_7$ (*2, 3*), $PbBi_2Te_4$ (*2*), $SnBi_2Te_4$ (*2*), $SnSb_2Te_4$ (*2, 4*), $GeBi_4Te_7$ (*2, 5*), $Ge Bi_2Te_4$ (*6*), $GeSb_2Te_4$ (*7*), and $GeSb_4Te_7$ (*8*). However, some of the structures determined from textured electron diffraction patterns (*3, 4*) have not been confirmed by X-ray diffraction (*2*).

It was proposed that in the compounds $Bi_{2+\delta}Te_3$ and $Bi_{2+\delta}Se_3$ excess bismuth is accommodated in the 15-layer structure by the periodic insertion of bismuth double layers (*1, 9*). However, this model does not seem to provide a satisfactory explanation of the observations (*1, 10*).

"Modulated structures" in Ge-doped Bi_2Te_3 were reported by Predota *et al.* (*11*). Some uncertainty remains concerning the way germanium is incorporated in these compounds. In this paper we will show that the structures in the system (Bi, $Ge)_{2+\delta}Te_3$

0022-4596/90 $3.00

Copyright © 1990 by Academic Press, Inc.
All rights of reproduction in any form reserved.

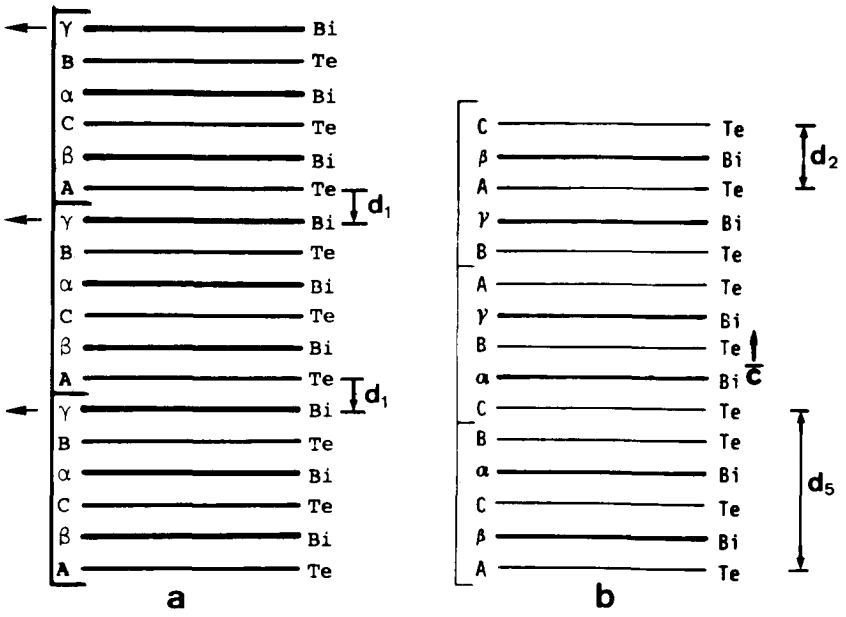

FIG. 1. Schematic representation of (a) the BiTe and (b) the Bi_2Te_3 structure.

can be considered as one-dimensional quasi-crystals built from two structural units, i.e., two types of lamellae with different thicknesses.

2. Structural Considerations

The structures of compounds of the type M_2X_3, such as Bi_2Te_3, can be represented by the stacking symbol (Fig. 1b)

$$A\beta C\alpha B\ C\alpha B\gamma A\ B\gamma A\beta C\ A. \ . \ . \quad (1)$$

The capital letters represent layers of tellurium atoms (X) and the Greek letters stand for layers of bismuth atoms (M). There are three five-layer lamellae in the repeat distance along the threefold axis, because the symmetry is rhombohedral. The bismuth atoms occupy the octahedral interstices in a cubic triplet of tellurium layers, forming ionically bonded five-layer lamellae. The five-layer lamellae themselves are held together predominantly by Van der Waals forces, but the bonding has also partly ionic character (*12*). Formally the structure can be considered to be an interface-modulated structure derived from the NaCl-type structure, the interfaces being the pseudo Van der Waals gaps. Extracting every sixth close packed bismuth layer from the (hypothetical) BiTe structure (2) and closing the gaps created in this way by a displacement over $\frac{1}{6}$ [0001], one obtains the structure represented below as (3) (Fig. 1a)

$$A\beta C\ \alpha B\gamma\ A\beta C\ \alpha B\gamma\ A\beta C\ \alpha B\gamma\ . \ . \ . \quad \text{(BiTe)} \quad (2)$$

$$A\beta C\alpha B\ A\beta C\alpha B\ A\beta C\alpha B\ . \ . \ . \quad (Bi_2Te_3). \quad (3)$$

Further shifting of successive five-layer lamellae over the vector $\frac{1}{3}[1\bar{1}00]$ results in the sequence (1), i.e., the observed structure represented by the stacking symbol "5" or 15R. The M_2X_3 structure can thus be derived from the NaCl-structure MX by shifting successive five-layer lamellae limited by X atom layers over a displacement vector $\frac{1}{6}$ [$2\bar{2}01$], when referred to the hexagonal description of the NaCl-type structure. In the

structure so formed, the stacking mode is cubic, but the separation of successive atom layers is modulated with the five-layer period (*13*).

Similarly one can generate from the MX compound a structure with composition M_3X_4 by extracting every eighth M layer and closing the created gap in the same way as described above. One thus obtains a 21-layer rhombohedral structure consisting of three seven-layer lamellae represented by "7" or 21R.

Structures with a composition intermediate between those of M_2X_3 and M_3X_4 can formally be obtained by mixing M_2X_3 and M_3X_4 lamellae in the appropriate proportions. We shall present evidence that this happens in compounds such as $Bi_{2+\delta}Te_3$, $Bi_{2+\delta}Se_3$, and $(Bi, Ge)_{2+\delta}Te_3$. It is furthermore possible to extend at least formally this kind of reasoning to the formation of nine-layer lamellae with a composition M_4X_5 and also, for decreasing M content, to structures MX_2 of the cadmium iodide type.

3. Sample Preparation

Compounds with overall compositions $(M, Ge)_{2+\delta}X_3$ and $M_{2+\delta}X_3$, $0 \leq \delta \leq 0.4$, were synthesized by mixing the constituent elements, subsequent melting in a quartz tube, annealing during 5–8 days at 400–450°C, and quenching to room temperature. Samples suitable for electron microscopy were obtained by depositing crushed material on copper grids dipped in glue. Generally, the as-prepared compounds were found to be inhomogeneous, containing different superstructures. Variation of the annealing conditions did not significantly improve the homogeneity of the samples.

4. Diffraction Patterns

4.1. The Bi_2Te_3 Structure

We shall now illustrate how the diffraction pattern of Bi_2Te_3 can be related to that of the NaCl-type structure, based on the formal way of deriving the structure of Bi_2Te_3 from that of BiTe as described above. According to the literature, BiTe and BiSe can adopt the NaCl-type structure (*14*). However, our results are independent of the actual occurrence of this structure for BiTe.

The reasoning is based on the geometry of the diffraction pattern of an interface-modulated structure. For such a structure the superstructure spots arise at positions given by (*15*)

$$\mathbf{g} = \mathbf{H} + 1/d\,(m - \mathbf{H} \cdot \mathbf{R})\mathbf{e}_u, \qquad (4)$$

where $\mathbf{H}$ describes the positions of the spots caused by the basic structure (i.e., the unshifted structure); d is the average distance between the interfaces, which are assumed to be all of the same type and which have a displacement vector $\mathbf{R}$; $\mathbf{e}_u$ is the unit vector perpendicular to the interfaces; m is an integer.

The $[10\bar{1}0]$-zone diffraction pattern of Bi_2Te_3 is shown in Fig. 2a. The distance between the most intense spots along the [00.1]* row corresponds to the average interlayer spacing $d_1 = 0.2032$ nm. The distance between the weaker superlattice spots corresponds with an interplanar spacing equal to the thickness of the five-layer lamellae, i.e., $d_5 = 1.01$ nm. The second and third reflections in the sequence are the most intense superlattice reflections. These features can be understood, at least qualitatively, by the fractional shift method on which the expression (4) is based.

The basic NaCl-type structure would produce a $[10\bar{1}0]$ zone pattern with spots at the positions indicated by crosses in Fig. 2b. The central $000l$ row perpendicular to the layer planes would exhibit spots at $\mathbf{H}_0 =$ 0002 (corresponding to $d_1 = 1/H_0$) and at 0001 (corresponding to $d_2 = 2d_1$).

The superstructure generated from the NaCl-type structure in the way described will produce sequences of equidistant superstructure spots, their spacing being $1/d_5$

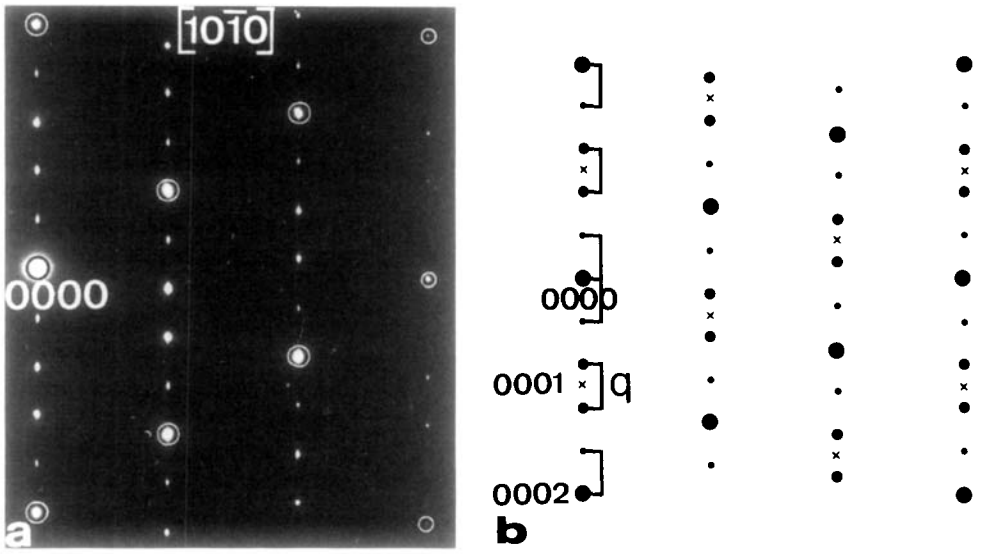

FIG. 2. (a) Diffraction pattern of pure Bi_2Te_3. (b) Schematic representation of the diffraction pattern shown in (a). Small, medium, and large dots correspond to the Bi_2Te_3 pattern. Large dots and crosses correspond to the BiTe pattern.

$= (\frac{1}{5})\ (1/d_1)$. Along the *000l* rows the fractional shifts $\mathbf{H} \cdot \mathbf{R}$ are 0 (mod 1) for $\mathbf{H}$ = 0000, 0002, and $\frac{1}{2}$ (mod 1) for $\mathbf{H}$ = 0001, 0003. The second and third spots can be considered as being generated by the symmetrical splitting of the 0001 spot, the magnitude of the splitting being given by $q = (\frac{3}{15})\ (1/d_1) = 1/d_5$ and the fractional shift by $\frac{1}{2}$. The first and fourth spots are derived from the basic spots 0000 and 0002 by a shift over 0 (mod 1) of the same magnitude q. These relationships are shown schematically in Fig. 2b. The second and third spots are more intense than the first and fourth because the former are closer to the positions of the associated basic 0001 spot than the latter to the 0000 and 0002 spots (*15*). The $h\bar{h}0l$ rows of spots all have the same geometry as the *000l* row, but they are shifted by $\frac{1}{3}$ of the interspot spacing along the c^*-direction, in agreement with the displacement vector and with the rhombohedral symmetry.

This somewhat formal way of interpreting the diffraction pattern of Bi_2Te_3 may look unnecessarily complicated; however, the same method "mutatis mutandis" also allows us to interpret the more complex superstructure diffraction patterns, commensurate as well as incommensurate.

4.2. Commensurate Diffraction Patterns in (Ge, Bi)$_{2+\delta}$Te$_3$, Bi$_{2+\delta}$Te$_3$, and Bi$_{2+\delta}$Se$_3$

We shall first discuss the diffraction patterns due to commensurate structures. The diffraction patterns along the zone perpendicular to the cleavage plane do not exhibit any superlattice spots in any of the compounds, suggesting that the germanium atoms in the germanium-containing compounds are either distributed at random in the layer planes or that they occur as complete close-packed layers, parallel with those of the parent structure. Since there is evidence for superstructure formation from diffraction patterns along other zones, also in the compounds with excess Bi, we conclude that presumably the Ge (or the excess Bi) are taken up either as full layers or that

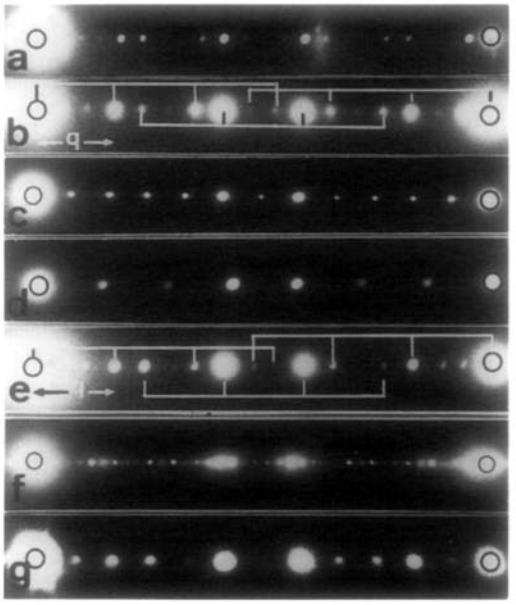

FIG. 3. Central rows (*000l*) of the diffraction patterns of different commensurate phases in the $(Bi, Ge)_{2+\delta}Te_3$ system. (a) 66R with stacking sequence "5557." (b) 51R with stacking sequence "557." (c) 12H with stacking sequence "57." (d) 21R with stacking sequence "7." (e and f) Incommensurate patterns. (g) (*000l*) Row of the 12H phase in $Bi_{2+\delta}Se_3$. The q-value is indicated in (b) and (e).

Ge is incorporated in the Bi-layers in a random fashion.

Representative *000l* rows of diffraction spots for different phases are represented in Fig. 3, whereas a complete diffraction pattern along $[10\bar{1}0]$ for one of the structures is shown Fig. 4a. We shall analyze only the latter pattern in detail, the others being analogous. The most intense spots still correspond with an interlayer spacing d_1. The interspot distance 0000–0002 is divided into 17 equal intervals by superstructure spots in the manner shown schematically in Fig. 5c. Moreover, superstructure spot sequences in rows parallel to c^* (Fig. 4a) are shifted by $\frac{1}{3}$ of the interspot separation as indicated by white lines, showing that the superstructure is rhombohedral, as is the basic structure (Fig. 2). In Fig. 5c we have indicated by crosses the positions of the spots caused by the basic Bi_2Te_3 structure. It is clear that the most intense superstructure reflections occur close to spot positions of the basic structure. The linear sequences of superstructure spots connected by brackets in Figs. 5a and c are fraction-

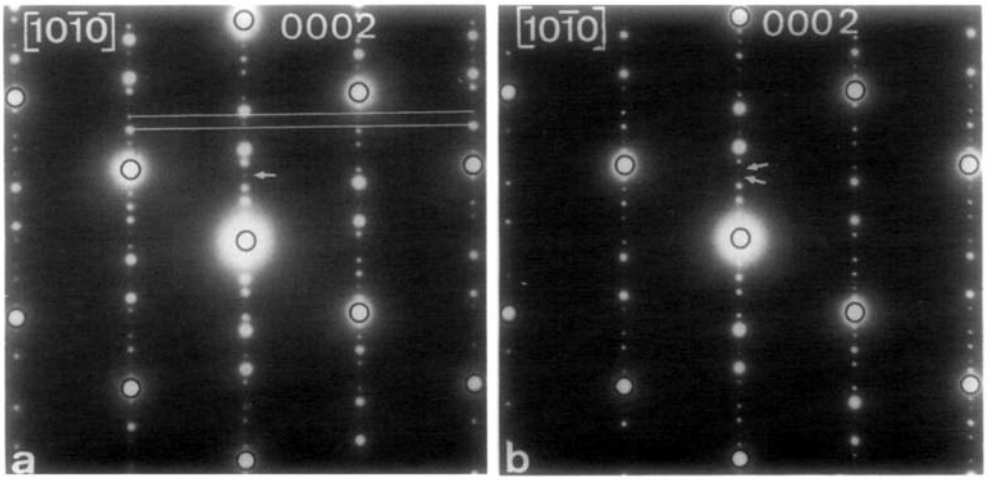

FIG. 4. (a) Diffraction pattern of the 51R phase in $(Bi, Ge)_{2+\delta}Te_3$ along a zone parallel with the close packed rows of atoms. Note that the distance between two basic spots is divided in 17 intervals. (b) Diffraction pattern along the same zone of the 138R phase. The pattern is pseudo-incommensurate.

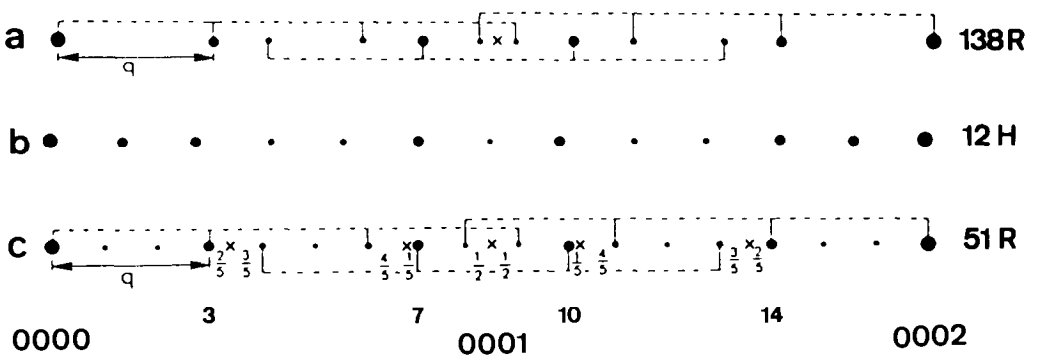

FIG. 5. Schematic representation of the (*0001*) row of some diffraction patterns of Figs. 3 and 4: (a) 138R; (b) 12H; (c) 51R. The respective q-values and the satellite sequences are indicated.

ally shifted with respect to these basic spots; the fractions are indicated. These observations suggest that the superstructure still predominantly consists of five-layer lamellae of the Bi_2Te_3 structure, which are displaced one relative to the next over **R** such that **H** · **R**, the fractional shift at **H**, is equal to the observed fractional shift at the reflection **H** of the "basic" structure which is now the M_2X_3 structure. The component of **R** along the c-axis can be deduced immediately from the observed shifts. Let **R** $[u\ v \cdot w]$ be the displacement vector referring to the superlattice. Then for **H** = 0003 (M_2X_3), we must have **H** · **R** = $3w = \frac{2}{5}$; i.e., $w = \frac{2}{15}$. This value of w also leads to the observed fractional shifts for all reflections in the sequence. Since the basic structure contains 15 layers, this shift corresponds to the insertion (or the extraction) of 2 layers. High resolution images (to be discussed below) indicate that the stacking mode of all layers, including the inserted one, remains cubic. Inserting 2 layers is thus only possible if at the same time also a relative shear between two lamellae over $\frac{1}{3}$ $[1\bar{1}00]$ occurs (referred to a hexagonal reference frame).

In the literature it is suggested that in $Bi_{2+\delta}Te_3$ and in $Bi_{2+\delta}Se_3$ compounds a continuous series of phases is formed, accommodating the excess bismuth atoms as double Bi-layers inserted between the 5-layer lamellae (*1*, *9*). On the other hand, in the Ge-containing compounds it is suggested that 7-layer lamellae occur with a layer sequence Te–Bi–Te–Ge–Te–Bi–Te in a 21-layer rhombohedral structure (*7*). One could imagine the excess bismuth being incorporated in a similar way, i.e., by the formation of 7-layer lamellae Te–Bi–Te–Bi–Te–Bi–Te (and similar for the Bi–Se system). Both models introduce two excess layers between the M_2X_3 lamellae and thus give rise to the same observed fractional shifts and to the formation of 5- and 7-layer lamellae. In one case a bismuth double layer is inserted to form the 7-layer lamellae, in the other case a BiTe layer is inserted. The 7-layer lamellae therefore have different compositions, i.e., $Bi_2Te_3 + Bi_2 = Bi_4Te_3$ and $Bi_2Te_3 + BiTe = Bi_3Te_4$, respectively.

Assuming the "Bi_2" model, the 17-layer sequence for the 51R structure is

Te Bi Te Bi Te
5
Te Bi Te Bi Te
5
Te Bi Te Bi Te Bi Bi,
7

whereas for the "BiTe" model the sequence is

Te Bi Te Bi Te
5
Te Bi Te Bi Te
5
Te Bi Te Bi Te Bi Te.
7

Both sequences can be generated from the NaCl-type structure of BiTe by the periodic extraction of metal layers and closing of the gaps. For the first model the 6th and the 12th bismuth layers and the 19th tellurium layer have to be extracted from the NaCl-type structure. For the second model the 6th, the 12th, and the 20th bismuth layers have to be extracted. In both cases the displacement vector is $\frac{1}{6}[111]_{NaCl}$ for all interfaces and the average distance between the interfaces is also the same, i.e., $17/3d_1$ (the q-value is $\frac{3}{17}(1/d_2)$). The geometry of the $[hk \cdot 0]$ diffraction patterns will thus be the same for the two models. In the "BiTe" model the midplanes of the lamellae are mirror planes in the sequence, whereas in the "Bi_2" model this is not the case. Moreover, in the latter case it is not clear to which of the two adjacent 5-layer lamellae the Bi_2 layers have to be attached in order to form the 7-layer lamellae. It is thus not possible to distinguish between "557557 . . ." and "755755 . . . ," but this is irrelevant anyway since these sequences represent the same structure.

Without deciding at this stage between the two models, we can analyze the observed diffraction patterns in terms of structures built from two basic units: a five- and a seven-layer lamella.

In all (commensurate) diffraction patterns discussed so far, the distance between the spots 0000 and 0002 of the basic NaCl-type structure is divided into a number of intervals which can be written as the sum of 5s and 7s. The *000l* rows of some observed patterns are reproduced in Fig. 3; for some of them the q-value is indicated; the number of intervals is 5 (Fig. 2), 7 (Fig. 3d), 12 (Fig. 3c), 17 (Fig. 3b), and 22 (Fig. 3a), respectively. This suggests that a description of the structures in terms of 5- and 7-layer lamellae is meaningful. In particular in Fig. 3b the distance between 0000 and 0002 is divided into 17 equal intervals. The spots "7" and "10" are the most intense ones, because they are closest (at a distance $[\frac{1}{2}]q$) to the 0001 spot positions (marked by crosses in Fig. 5c) from which they are derived. The fractional shift is thus $\frac{1}{2}$ (mod 1) for $\mathbf{H} = 0001$. The spots "3" and "14" are the second most intense ones because they are satellites derived from the basic spots 0000 and 0002, but they are separated from these spots by a distance q, i.e., the fractional shift is 0 (mod 1). The intensities of all superstructure spots in a sequence (connected by brackets in Figs. 3 and 5) decrease with increasing separation from the basic spot from which they are derived. This is in accordance with the predictions of the theory on which the fractional shift method is based (*15*). These considerations allow us to deduce the q-vector; in the *000l* row this vector joins the origin with the first intense satellite. The same q-vector also connects the two symmetrically located intense spots around the 0001 positions. The diffraction patterns of the other commensurate phases have the same general characteristics as the 51R pattern. Some of the patterns are represented schematically in Fig. 5, in which also the fractional shifts are indicated; the fractional shifts are the same for all phases, but the interspot separations in the satellite sequences, i.e., the q-values, are of course different for the different phases.

In some germanium-rich compounds commensurate diffraction patterns such as the one shown in Fig. 6b were found. The distance between 0000 and 0002 is now divided in nine intervals; i.e., within experi-

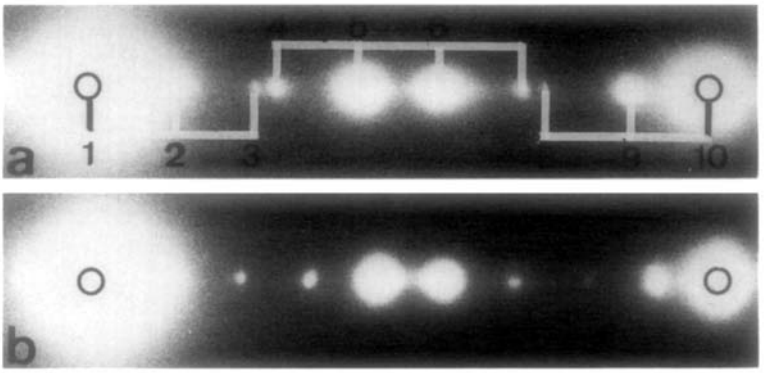

FIG. 6. (a) Central row of a pseudo-commensurate pattern observed in the same specimen as (b). The measured q-value is about $\frac{4}{15}$. (b) Central row (*000l*) of a commensurate pattern in a Ge-rich specimen. The distance between basic spots is divided in nine intervals, suggesting a $(Bi, Ge)_4Te_5$ structure.

mental error one finds $\mathbf{q} = (\frac{1}{9})\mathbf{H}_0$. This suggests the existence of nine-layer lamellae. The most obvious explanation is to consider lamellae with the following sequence

$$X\text{–}M\text{–}X\text{–}M\text{–}X\text{–}M\text{–}X\text{–}M\text{–}X,$$

where the M layers contain germanium as well as bismuth. The positions and relative intensities of the spots are consistent with this interpretation; the two most intense spots symmetrically situated around the center again result from the splitting of the 0001 basic reflection.

4.3. Incommensurate Diffraction Patterns

Some of the patterns, such as that in Fig. 4b, can be indexed as commensurate patterns, but this would imply the use of a large repeat distance and moreover the monotonic decrease in intensity in the satellite sequences would not be obeyed. It is therefore more realistic to consider these diffraction patterns as incommensurate and based on a q-vector which is not very different from that found in the commensurate structures. The q-vector is indicated in Fig. 5a. A rational approximant is $\mathbf{q} = (\frac{4}{23})\mathbf{H}_0$. A hint as to the choice of the q-vector is provided by the separation of the two intense spots symmetrically located with respect to the center (i.e., the 0001 basic position) of the satellite sequence. The pattern is analyzed further below.

In the germanium-rich compounds in which the ninefold period was discovered, one also finds incommensurate patterns of the type reproduced in Fig. 6a. The intersatellite spacing within a sequence is smaller than $(\frac{1}{7})\mathbf{H}_0$; it is thus not possible to construct a sequence based on five- and seven-layer lamellae and have an average spacing that would lead to the observed interspot spacing. Therefore it is necessary to introduce lamellae with more than seven layers. As a consequence, it seems reasonable to mix seven- and nine-layer lamellae. We discuss this case further below.

5. High Resolution Images

High resolution images were obtained along the close-packed directions in the close-packed layer planes; in this way atom columns can be imaged as bright (or dark) dots and the layer stacking can be deduced directly from the images. Both Bi and Te atom columns are imaged. Along the directions 1 and 2 indicated in Figs. 7 and 8, the rows of bright dots are straight, showing that the stacking mode of the layers is cubic

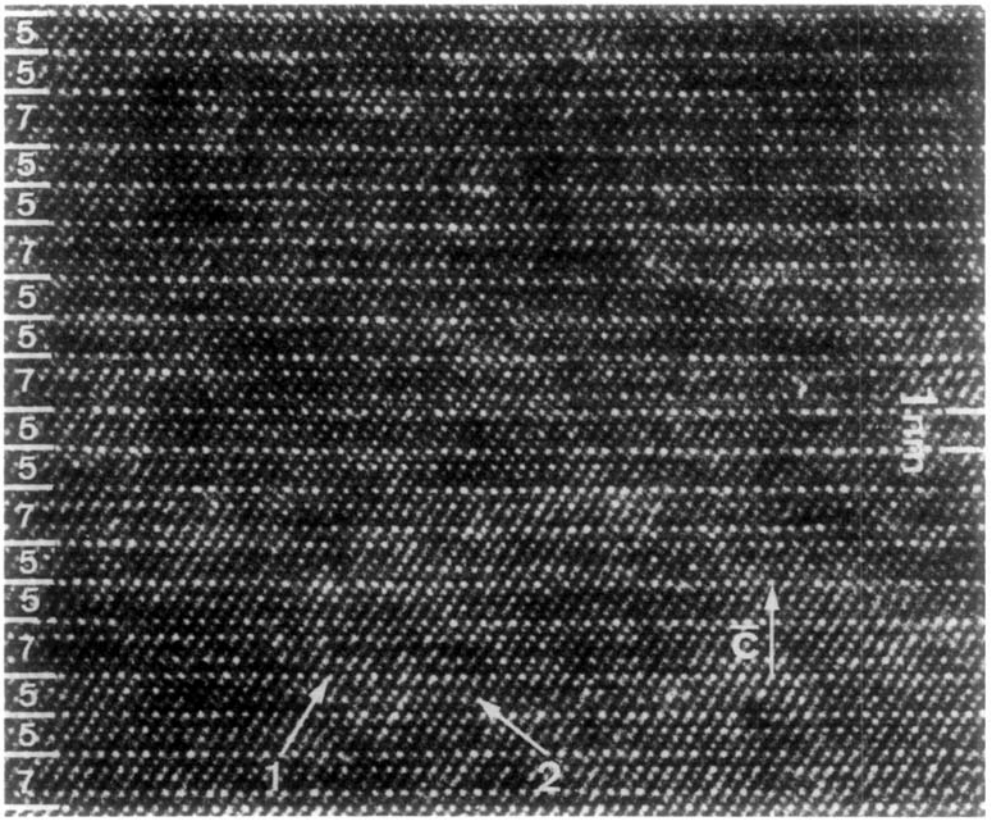

FIG. 7. High resolution image of the 51R phase (sequence "557").

close-packed. The image corresponding to a 51R diffraction pattern is reproduced in Fig. 7, and a more complicated sequence is reproduced in Fig. 8. It is clear that rows of extra-bright dots, forming bands with two different spacings, are present; they are indicated in both figures. The narrow bands contain four roughly equidistant rows of dots between the two outer rows of extra bright dots. The wide bands are often visibly separated in three narrow bands; they contain six roughly equidistant rows of bright dots between the two limiting rows of extra-bright dots. Among these six rows, two rows usually consist of somewhat brighter dots; these are separated from the limiting rows by one row of weaker bright dots.

Associating bright dots with atom columns, the narrow bands can be regarded as images of the five-layer lamellae (represented by the symbol "5") and the wider bands as images of seven-layer lamellae (represented by the symbol "7"). The succession of lamellae is clearly "557," whereas in Fig. 8 it is "55755757" with some faults, even though it is not always unambiguous which is the 5-band and which is the 7-band in adjacent bands. In this respect it is in fact often more convenient to limit intentionally the resolution and form a one-dimensional fringe pattern using a central row of *000l* reflections for imaging. Such a one-dimensional image is shown in Fig. 9, where 5- and 7-bands can clearly be distinguished as fringes with a different

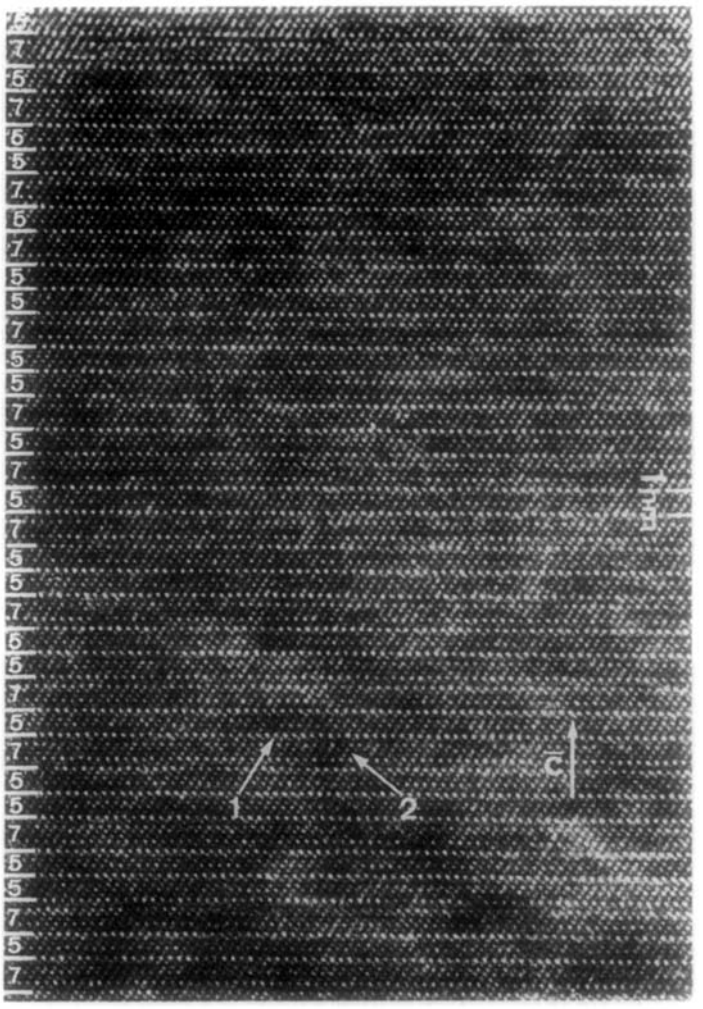

FIG. 8. High resolution image of the 138R phase (sequence "55755757") which produces the diffraction pattern of Fig. 4b.

spacing. The image of Fig. 9 represents the sequence "57" = 12H. Figure 10 shows a high resolution image along the same zone of the 12H phase in $Bi_{2+\delta}Se_3$ (the *000l* row of the corresponding diffraction pattern is reproduced in Fig. 3g). The image clearly exhibits the "5" and "7" lamellae which alternate in the 12H structure ("57"); this image also confirms the overall cubic stacking. Since Se and Bi have a larger difference in atomic weight than Te and Bi, the difference in brightness of the dots imaging the two kinds of atomic columns is expected to be larger in this case. The dots in $Bi_{2+\delta}Se_3$ have indeed two significantly different brightnesses in Fig. 10. This is consistent with the atomic column approximation (*16*). In a five-layer lamella there are two rows of bright dots sandwiched between three rows of less-bright dots, whereas in the seven-layer lamellae there are three rows of bright dots sandwiched

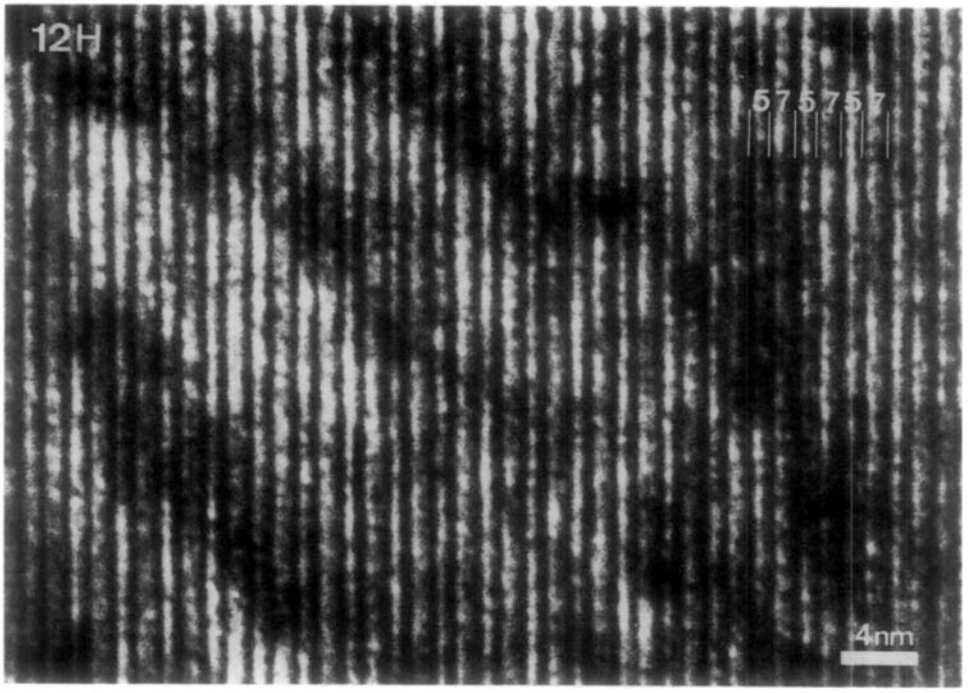

FIG. 9. Lattice image of the 12H phase, wide ("7") and narrow ("5") bands alternate.

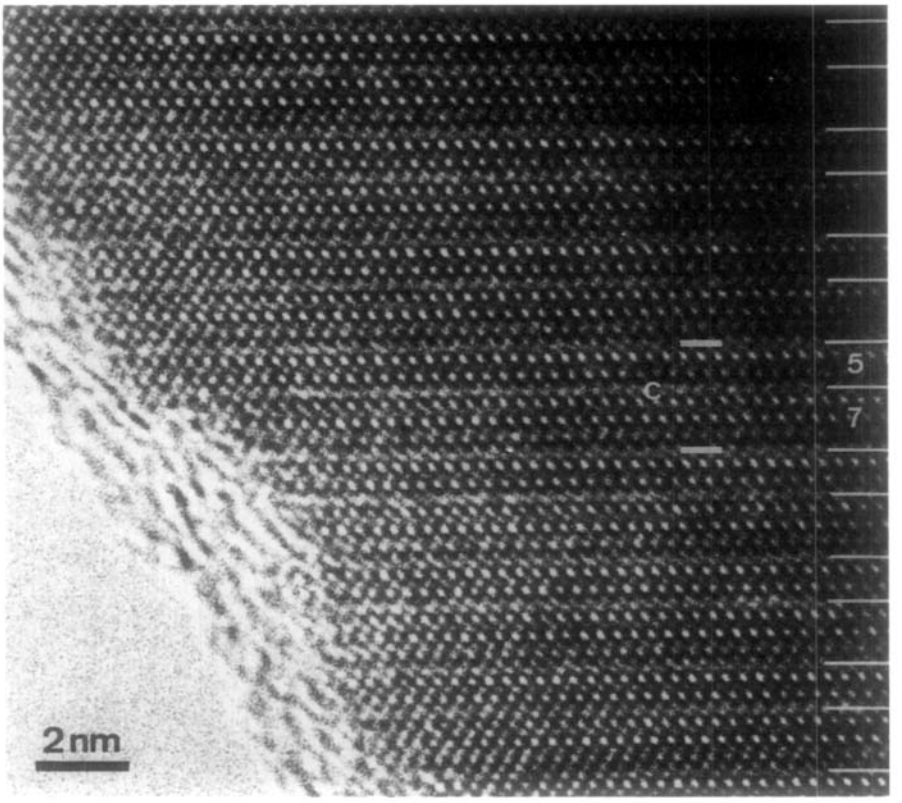

FIG. 10. High resolution image of the 12H ("57") phase in $Bi_{2+\delta}Se_3$. All atom columns are resolved; the brightest dots image Bi columns.

between four rows of less-bright dots. Such an image can consistently be interpreted only if the brightest dots are associated with Bi columns and the less-bright dots with Se columns. These observations were made in a compound with nominal composition Bi_9Se_{13}. After a long annealing treatment ($2w$ at 350°C) we obtained predominantly the 12H phase. With the 5-bands having the composition Bi_2Se_3 and the 7-bands the composition Bi_3Se_4, the overall composition of the 12H structure would be Bi_5Se_7 or $Bi_9Se_{12.6}$. If on the other hand the 7-band contains a Bi double layer, its composition would be Bi_4Se_3 and the overall composition of the 12H structure would be Bi_6Se_6. It is quite evident that the central layer model leads to a composition which is much closer to the macroscopic composition than the Bi double layer model. However, according to the macroscopic composition, the expected structure should be "5557." The excess selenium in Bi_9Se_{13} is possibly present in separate 5-lamellae, the material being two-phase "57" + "555." Alternatively, antistructure defects may be present. In $Bi_{2+\delta}Se_3$ the 12H phase seems to be particularly stable, since it is apparently found in a wide composition range; this is the subject of further research.

The high resolution images thus strongly support the assumption that the diffraction patterns have to be interpreted in terms of five- and seven-layer bands. The phases discussed here form a simple model system producing structures consisting of lamellae with two different thicknesses (5 and 7) and in which the relative abundances of the two types of lamellae are composition-dependent.

6. Derivation of Layer Sequences

Sequences of lamellae of two different thicknesses l(arge) and s(mall) can give rise to diffraction patterns consisting of sharp spots, provided such sequences are generated by an appropriate algorithm, ensuring the best approximation to an equidistant sequence which can be achieved with the two types of lamellae. Such an algorithm is well known for ordered alloys, where use is commonly made of the Fujiwara square wave method to derive the stacking sequence of cubic unit cells with a cell edge a_0, belonging to a given M-value and consisting of bands with widths ma_0 and $(m + 1)a_0$ (m is an integer) (*17*). In the present case this algorithm does not apply. In 1D superstructures consisting of two different lamellae with arbitrarily related thicknesses, an algorithm was described by Katz and Duneau (*18*) for quasi-crystals, and by several other authors (e.g., *19, 20*). We shall describe here a related approach which can be applied to incommensurate as well as to commensurate sequences. It is based on a geometrical construction in 2D. In direct space the construction proceeds as follows (Fig. 11):

(i) Construct a lattice with a rectangular unit mesh based on (**a**, **b**). In this particular case $|\mathbf{a}| = s = 5$ and $|\mathbf{b}| = l = 7$ units (or 7 and 9 units); but s/l can be incommensurate.

(ii) Generate a "strip" by translating one such rectangle along a line with a direction enclosing an angle α with the a-direction, Figs. 11a, 11b, and 11c. This angle α is related to the q-value deduced from the experimental diffraction pattern through the relation (see Appendix for the derivation of this expression):

$$\alpha = \arctan\{-[l(qs - 1)]/[s(ql - 1)]\}. \quad (5)$$

(iii) Construct a zig-zag path by connecting the lattice points within this strip, approximating in this way in the best possible manner a straight line with slope α, through the origin. The points are allowed to coincide with one of the limiting lines of the strip only; Figs. 11a, 11b, and 11c.

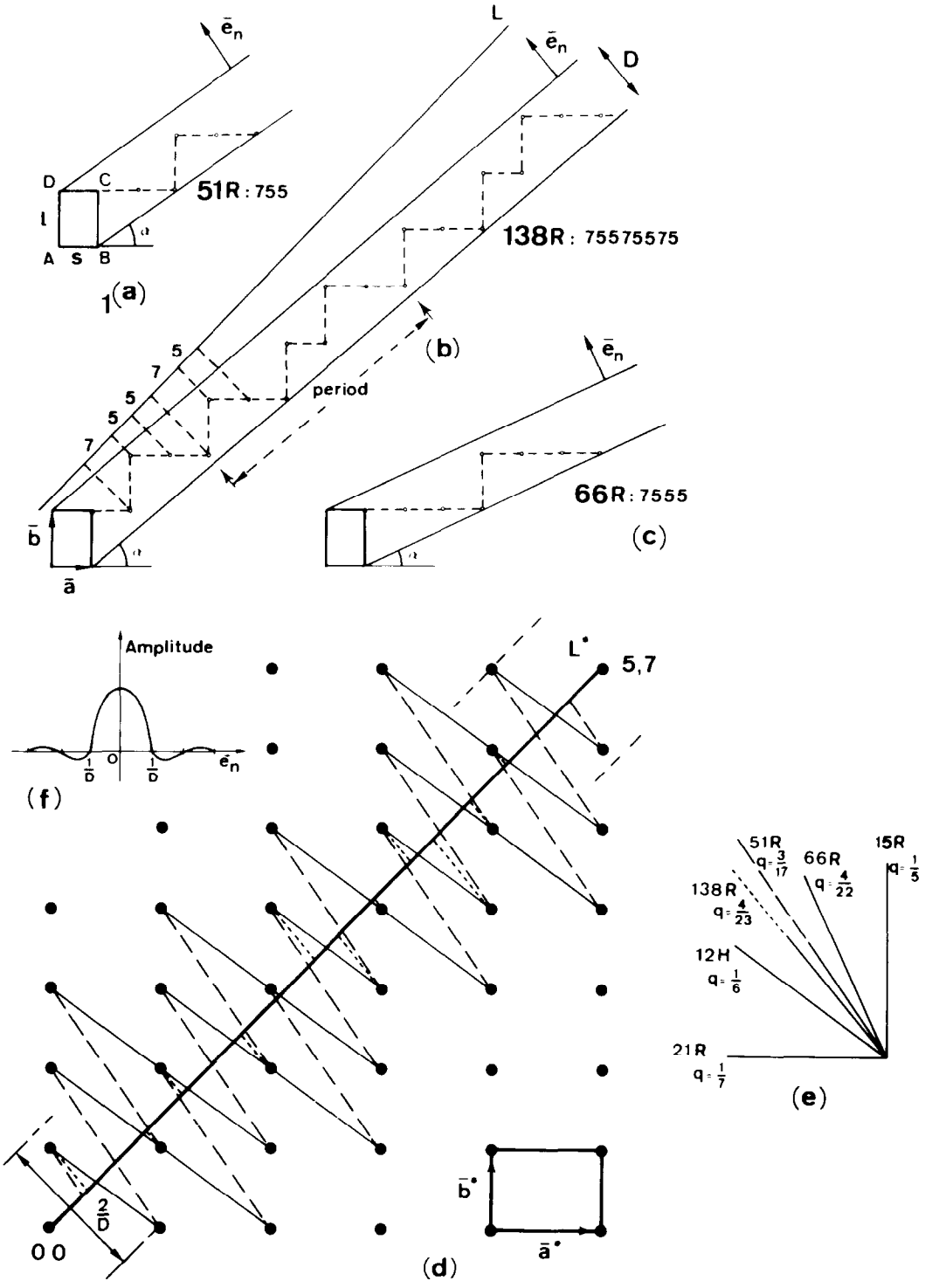

FIG. 11. (a) Geometrical construction used to derive the stacking sequences of the five- and seven-layer lamellae for the different q-values observed: (a) 51R: "557," $\mathbf{q} = (\frac{3}{17})\mathbf{H}_0$; (b) 138R: "57557557," $\mathbf{q} = (\frac{4}{23})\mathbf{H}_0$; (c) 66R: "5557," $\mathbf{q} = (\frac{4}{22})\mathbf{H}_0$; (d) Construction of the positions and the relative intensities of the diffraction spots of the patterns caused by the different phases. The directions of the lines (e) along which the slit function extends on both sides of each reciprocal lattice point is indicated for the different phases. The full line produces the 12H pattern; the dashed line the 51R pattern; the dotted line the 138R pattern. The width of the strip containing the nodes giving rise to observable spots is indicated for the 138R phase. (f) The shape of the slit function.

(iv) Project orthogonally the lattice points within this strip on a line L such that domains with the required ratio of sizes are obtained. In our geometry this line must enclose an angle of 45° with the a-direction in order to preserve the ratio 5:7. One thus obtains the desired succession of $l(7)$ and $s(5)$ domains; Figs. 11a, 11b, and 11c.

As a simple application, Fig. 11a illustrates the derivation of the sequence corresponding to $\mathbf{q} = (\frac{3}{17})\mathbf{H}_0$ and thus $\alpha = \arctan(0.7)$, $H_0 = 1/d_1$. This leads to the 17-layer sequence "557" or 51R. The construction leading to the 22-layer sequence "5557" or 66R is represented in Fig. 11c. In Figs. 3e and 5a, the *000l* row of an apparently incommensurate diffraction pattern is reproduced; it is indicated by brackets how the different satellite sequences are connected with the basic spots. The fractional shifts with respect to the NaCl-type basic structure are the same as in the commensurate case, but the q-value is different of course. Within experimental error, $\mathbf{q}$ can be approximated by the fraction $(\frac{4}{23})\mathbf{H}_0$, leading to $\tan\alpha = \frac{21}{25}$. The sequence predicted by the algorithm is then as represented in Fig. 11b, i.e., "57557557," and it is periodic. This is of course a consequence of the fact that we have approximated q by a rational number. The structure is rhombohedral and the unit cell contains $46 \times 3 = 138$ layers. The high resolution image of Fig. 8, which corresponds to this diffraction pattern, clearly exhibits the sequence deduced above. There are occasional deviations which can be understood by noting that q was approximated by a rational number, whereas in actual fact q is presumably incommensurate.

7. Theoretical Diffraction Patterns

The "strip" method allows us to interpret not only the geometry but also the relative spot intensities in the diffraction pattern. The present system is to the best of our knowledge the first 1-D system that gives rise to commensurate and incommensurate superstructures containing lamellae with two arbitrarily differing thicknesses. In order to obtain the diffraction pattern of the 1-D sequence, we have to transform to reciprocal or Fourier space the operations performed in direct space (section 5). Translating this construction into reciprocal space leads to the following operations (Figs. 11d and 11e):

(i) Construct the 2-D reciprocal lattice ($\mathbf{a}^*$, $\mathbf{b}^*$) of the 2-D lattice based on ($\mathbf{a}$, $\mathbf{b}$).

(ii) This reciprocal lattice must be convoluted with the Fourier transform of the infinitely long strip with width D. This Fourier transform is a delta function in the direction parallel to the slit, and it is a function of the type $[\sin \pi Dx/\pi Dx]e_n$ along the direction normal to the slit (e_n: unit normal to the direction of the slit). The shape of this curve is shown in Fig. 11f. The reciprocal lattice must be convoluted with this function, which means that such a function is now centered on each reciprocal lattice point. With each such node an intensity distribution has to be associated given by $A_g^2[\sin \pi Dx/\pi Dx]^2$, with the x-axis along e_n and where A_g can be shown to be proportional to the structure factor associated with the reciprocal lattice node under consideration (*21*).

(iii) The projection in direct space onto the line L becomes the intersection with the line L^* in reciprocal space. The line L^* connects the origin with the reciprocal lattice node (5, 7), i.e., it encloses an angle of 45° with the a^*-axis and is thus parallel to L. The line L^* intersects the intensity distributions which are centered on each node and which are only nonzero along lines normal to the slit directions. The further the intersection point with L^* is away from the node, the smaller in general the intensity of the corresponding diffraction spot.

The positions of the diffraction spots are thus obtained by projecting the reciprocal lattice nodes onto the line L^* along e_n, a direction perpendicular to the slit. This direction is different for different sequences, i.e., for different q-values. The projection directions corresponding to the different stacking sequences, i.e., the different q-values, are indicated in Fig. 11e.

Because of the shape of the Fourier transform of the slit (Fig. 11f), the intensities of the spots will, in the kinematical approximation, decrease with increasing distance of the reciprocal lattice nodes from the line L^*. Only nodes close to the line L^* will produce visible spots. Along commensurate directions, corresponding to rational q-values, several nodes project at the same position on the line L^* and the density of spots is small. Along incommensurate directions, corresponding to irrational q-values, the density of the diffraction spots can become very large; in fact the spots form a dense set, but only the most intense ones will show up in the diffraction pattern.

The dotted lines in the drawing of Fig. 11d refer to the particular case of the sequence 138R; it is clear that the positions as well as the relative intensities of the different diffraction spots are in surprisingly good agreement with the observations of Fig. 4b.

When projecting along the direction marked 51R (dashed line in Fig. 11d), one obtains 16 intermediate and equidistant spots; the relative intensities of the experimental pattern (Fig. 4a) are well reproduced. The same applies to the 66R sequence (Fig. 3a). One can also simulate the limiting case 21R by projecting along the a^*-direction. One then obtains a pattern consisting of six intermediate equidistant spots. Also the diffraction pattern of the five-layer case Bi_2Te_3 is well described; the second and third spots are the most intense ones, as observed.

The pattern of Fig. 6b leads to $q \approx \frac{2}{15}$. The construction of Fig. 12a using this value gives the sequence "7779." This is presumably a rational approximant only since in reality the structure may be incommensurate. The diffraction pattern derived by the method described above (Fig. 12b) is reproduced in Fig. 12c; it agrees quite well with the experimental pattern.

8. Image Simulations

In order to obtain information concerning the distribution of the germanium atoms over the different layers in the $(Bi, Ge)_{2+\delta}Te_3$ system and in particular to find out whether the Ge atoms occur in separate layers or are statistically distributed over the M-layers, image simulations were performed for comparison with experimental high resolution images. It has been established that the brightness of the image dots corresponding to the atom columns depends on the chemical composition of the columns; "mixed" columns are imaged differently from "pure" columns under appropriate imaging conditions (*22*). The images were computed by means of the fully dynamical real space method which also takes into account all instrumental parameters (*23*).

Two different models for the seven-layer bands in the phase ("57") were considered. In the first model, the germanium atoms were assumed to occupy the central layer of the seven-layer lamellae; i.e., the layer sequence is

$$/\text{Te–Bi–Te–}\underset{7}{\text{Ge}}\text{–Te–Bi–Te}\underset{5}{\text{Te–Bi–Te–Bi–Te}}/\ldots \quad (12H).$$

This model is inspired by the structure proposal for Bi_2Te_4Ge (*6*). In the second model, the germanium atoms are assumed to occupy statistically half of the sites in the

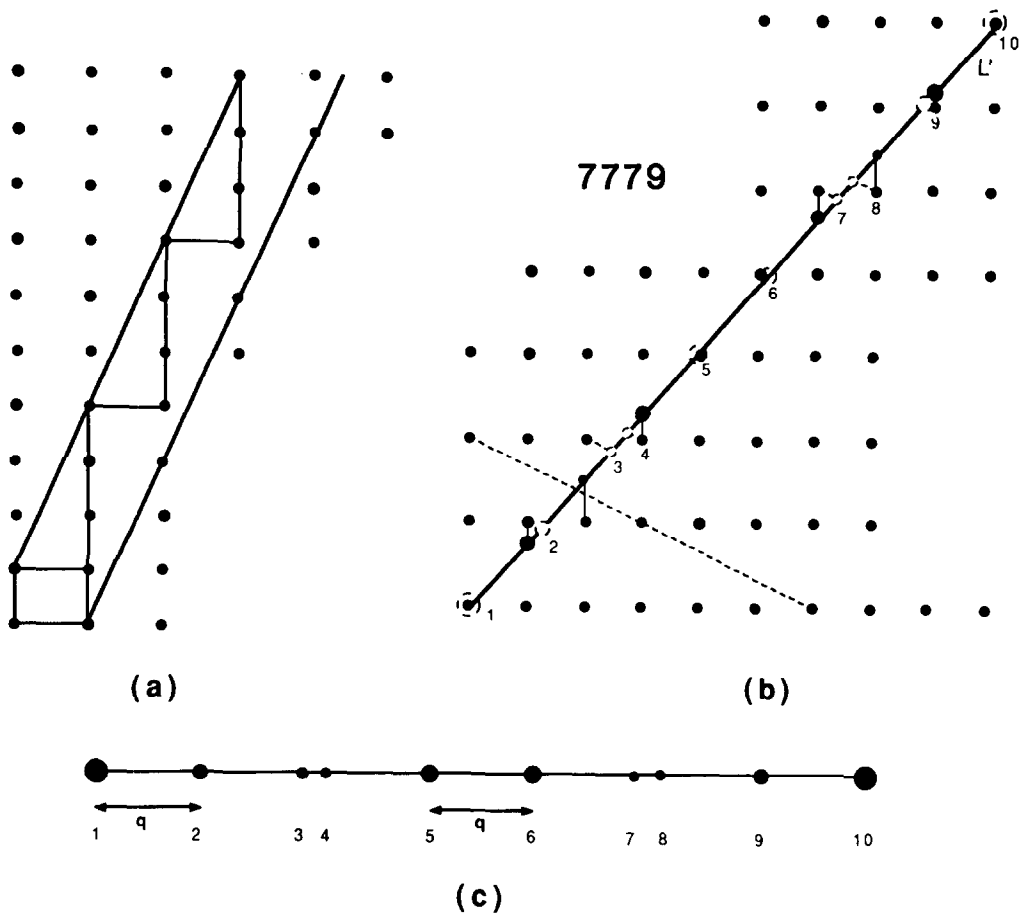

FIG. 12. Application of the method described in the text to the pattern in Fig. 6a. (a) The stacking sequence of seven-layer and nine-layer lamellae derived for $q = \frac{2}{15}$ is "7779." (b) and (c) Construction and representation of the corresponding theoretical diffraction pattern (to be compared with the experimental pattern in Fig. 6a).

two outer M-layers, i.e., the following sequence was used:

$$/\text{Te–(Bi, Ge)–Te–Bi–Te–(Bi, Ge)–Te}\ \underset{5}{7}\ \text{Te–Bi–Te–Bi–Te/}\ldots\ (12\text{H}).$$

A model with a statistical distribution of the Ge-atoms over all M-layers is considered to be improbable because the observed images suggest that the three M-layers in the seven-layer lamellae are not equivalent, since in the outer layers dots of a brightness different from those in the central layer are produced. Therefore, such a model was not considered further. We limited ourselves to "symmetrical" models because, under the appropriate conditions, the images have lines of symmetry along the central lines of the 5- and 7-bands.

The simulated images for the central layer model are represented in Fig. 13 for different thicknesses and different defocus values. The values of the instrumental parameters used in the simulation program were spherical aberration constant 1.2 mm;

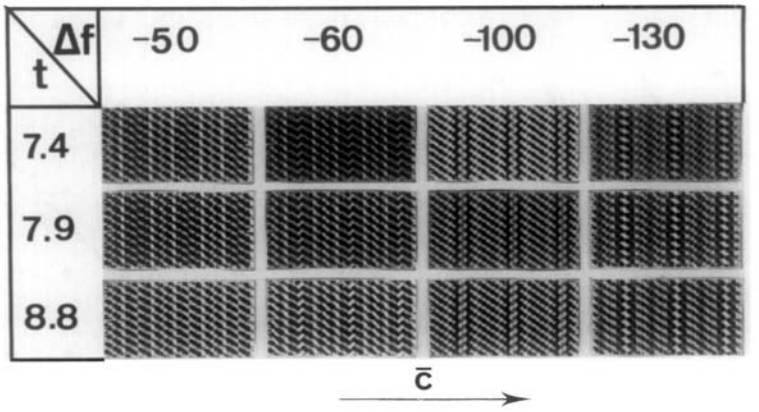

FIG. 13. Matrix of simulated HREM imagtes of the 12H structure for the "central layer" model; i.e., Ge occupies the central layer in the seven-layer lamellae.

half angle of beam divergence, 8×10^{-4} rad; defocus spread, 7 nm.

A matrix of computed images for the statistical model, under the same imaging conditions, is reproduced in Fig. 14, in which also the 12H unit cell is outlined. The tellurium atom adjacent to the pseudo-Van der Waals gap was put at the origin of the unit cell. This model was found to give the best fit with the experimental images, as is clear from Fig. 15, where computed images for different models for the 5- and 7-layer lamellae in the 12H structure are compared. The different images were calculated for the same instrumental parameters and imaging conditions (t = 7.4 nm, Δf = −60 nm) and corrrespond to the following models:

(a) . . ./Te Bi Te Bi Te/Te Bi Te Ge Te Bi Te/. . .

(b) . . ./Te Bi Te Bi Te/Te M Te Bi Te M Te/. . .

$$M = \tfrac{1}{2}(\mathrm{Bi} + \mathrm{Ge})$$

(c) . . ./Te Bi Te Bi Te/Te M_2 Te M_1 Te M_2 Te/. . .

$$M_1 = \tfrac{1}{2}(\mathrm{Bi} + \mathrm{Ge})$$
$$M_2 = \tfrac{3}{4}\,\mathrm{Bi} + \tfrac{1}{4}\,\mathrm{Ge}$$

(d) . . ./Te Bi Te Bi Te/Te M_3 Te M_3 Te M_3 Te/. . .

$$M_3 = \tfrac{2}{3}\,\mathrm{Bi} + \tfrac{1}{3}\,\mathrm{Ge}$$

(e) . . ./Te M_4 Te M_4 Te/Te M_4 Te M_4 Te M_4 Te/. . .

$$M_4 = \tfrac{4}{5}\,\mathrm{Bi} + \tfrac{1}{5}\,\mathrm{Ge}$$

It can thus be concluded that the Ge-atoms in the seven-layer lamellae are preferentially located in the outer M-layers and that they are statistically distributed over these layers. The variability in brightness of the dots in the corresponding rows is consistent with differences in composition of these columns.

9. Discussion

The relationship of the series of compounds $M_{2+\delta}X_3$ with the NaCl-type MX structure is not only formal in the case of BiTe and BiSe. The stoichiometric compounds apparently do not melt congruently and on slow cooling more complex structures than the NaCl-type structure are formed. However, on quenching one obtains a rhombohedrally deformed face-centered lattice with a = 0.65 nm, which is consistent with a deformed NaCl-type structure (*14*). The interpretation of the complex phases as derivatives of a NaCl-type structure thus seems reasonable.

The derivation of the layer sequences from the observed q-values is independent

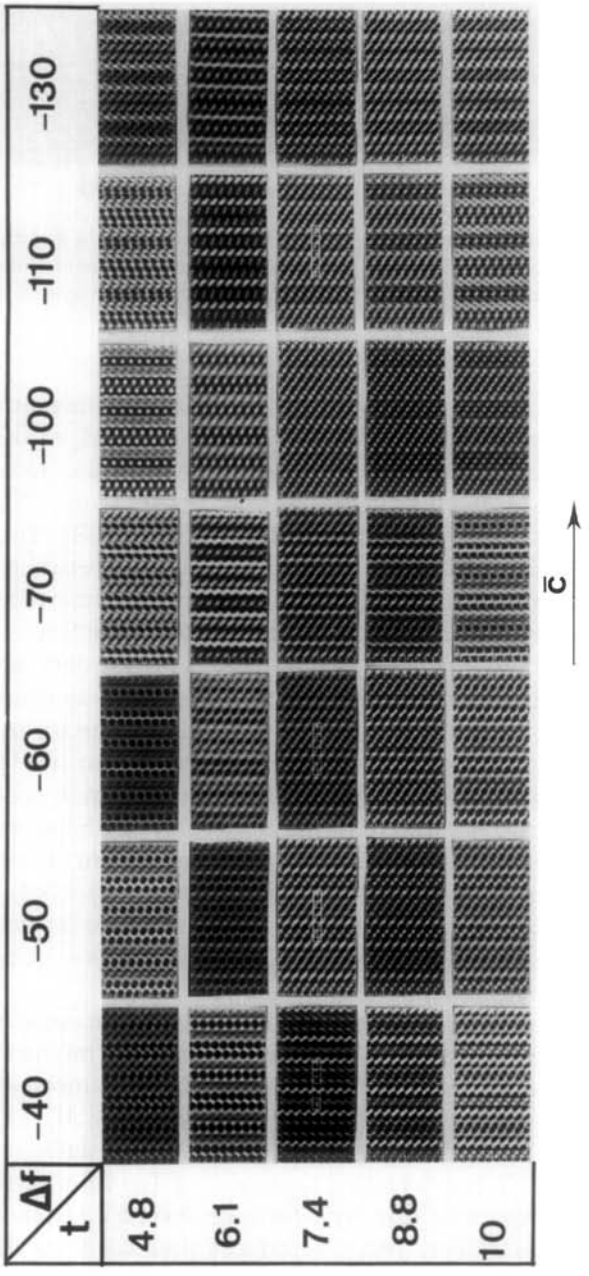

FIG. 14. Matrix of simulated HREM images of the 12H structure for the "statistical" model; i.e., Ge occupies half of the sites in the outer M-layers of the seven-layer lamellae. The unit cell of the 12H structure is outlined in one of the simulated images.

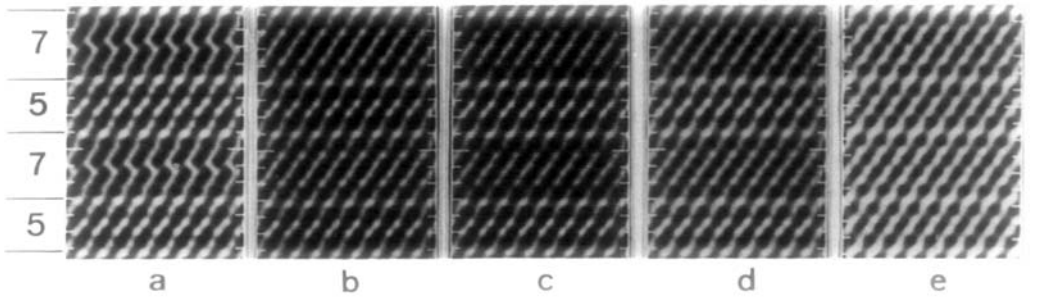

FIG. 15. Comparison between calculated images for different models for the distribution of cations in the 12H structure of the (Ge, $Bi)_{2+\delta}Te_3$ system. All images were calculated for $t = 7.4$ nm and $\Delta f = -60$ nm. Model (b) gives the best correspondence with the experimental images. See text for details concerning the different models.

of the detailed structure of the five- and seven-layer lamellae. Also the geometry of the diffraction patterns does not depend on the chemical compositions of the lamellae. However, spot intensities clearly depend on the actual structure. The *000l* rows of the kinematical diffraction patterns for the 12H and the 51R structures using a bismuth double layer on one hand and a symmetrical layer sequence for the seven-layer lamellae (Te–Bi–Te–Bi–Te–Bi–Te) on the other hand were calculated and compared with corresponding experimental patterns. Although electron diffraction is essentially dynamical, the relative intensities obtained from the very thin foils used for high resolution studies usually correlate well with the kinematically computed intensities. From such a comparison it can be concluded that the model containing symmetrical seven-layer lamellae leads to a better fit with the observed patterns than the model with the double bismuth layers.

The compounds $M_{2+\delta}X_3$ have composition-driven structures which can formally be derived from a NaCl-type structure by extracting M-layers, where M may represent either a pure Bi-layer or a mixed (Bi, Ge)-layer. In the composition range M_2X_3 to M_3X_4 the structures contain uniform mixtures of five- and seven-layer lamellae. The q-vector changes with composition in a quasicontinuous manner from $\mathbf{q} = (\frac{1}{5})\mathbf{H}_0$ in Bi_2Te_3 to $\mathbf{q} = (\frac{1}{7})\mathbf{H}_0$ in Bi_3Te_4. In this composition range the most frequently observed phases are "57" (12H), "557" (51R), "5557" (66R). There is no unambiguous correlation between the bulk composition and the theoretical composition associated with the structure. This is presumably because the powders are not completely equilibrated, the annealing times being finite. Perhaps a certain amount of antistructure formation may also explain this result.

In germanium-rich specimens diffraction patterns corresponding with structures consisting of a mixture of seven- and nine-layer lamellae were observed. Uniform mixtures of seven- and nine-layer lamellae can occur in the composition range from M_3X_4 to M_4X_5.

In principle one could extrapolate further and assume that mixtures of lamellae containing an odd number of layers will occur for compositions $M_{n+\delta}X_{n+1}$ with $n \to \infty$. However, it is unlikely that regular sequences of Te–Te interfaces will be formed for large average spacings between the interfaces, i.e., for thick lamellae.

The binary and pseudo-binary systems discussed here can be described as one-dimensional quasi-crystals, consisting in general of an alternation of blocks of two sizes, either 5 and 7 or 7 and 9, or perhaps even

mixtures containing blocks of larger sizes. In reality the ratio of the block sizes will not be a simple fraction such as $\frac{5}{7}$ or $\frac{7}{9}$, since the interlayer spacings are not all identical. Most of the observed structures can be generated by a Fibonacci-type algorithm applied to the 5- and 7-lamellae, ensuring hereby self similarity. The inflation rule is $5 \rightarrow 57$, $7 \rightarrow 5$ for the compounds close to 5 and $5 \rightarrow 7$, $7 \rightarrow 75$ for the compounds close to 7. The first algorithm generates the following sequences:

5	5	15R
5 7	57	12H
5 7 5	557	51R
57 5 57	55757	87R
57557575	55755757	138R

All of these sequences have been observed. However one of the simpler observed sequences, 66R with the stacking symbol 5557, is not generated by this algorithm. The first inflation rule in fact can only generate structures in which at most two consecutive 5-λ lamellae occur and where all 7 lamellae are isolated; and vice versa for the second inflation rule.

The successive blocks have the same orientation, but there will be no strict translational order except for rational q-values, i.e., for certain compositions. In all sequences found as yet, the minority domains occur isolated and if more than one group of five-layer lamellae occurs the number of five-layer lamellae in these groups differ by 1 unit only. These are characteristic features of "uniform" sequences producing sharp diffraction spots (*17*).

Previous authors noted that there is no simple relationship between the c-parameter, i.e., the length of the stacking sequence, and the composition for $Bi_{2+\delta}Te_3$ (*1*) nor for $(Bi, Ge)_{2+\delta}Te_3$ (*11*). According to the model presented here there is indeed not such a simple relationship, but there should be a monotonic decrease in the q-value, i.e., the average lamella thickness, with increasing value of δ. Since the length of the stacking sequence depends in a complicated manner on the q-vector and hence on the composition, so does the c-parameter.

It is interesting to note that also the rhombohedral, composition-driven, vacancy-ordered superstructures in the Al–Cu–Ni system (*24*), which are derived from a CsCl-type structure, can be considered as one-dimensional quasi-crystals. Their diffraction patterns (*24, 25*) can be analyzed in a similar fashion (*25*).

Appendix

The magnitude of q for a sequence containing n fivefold lamellae and m sevenfold lamellae is given by

$$1/q = (5n + 7m)/(m + n), \qquad (1)$$

irrespective of the succession in which the two kinds of lamellae appear in the sequence.

The slope of the pair of lines in Fig. 11 is likewise given by

$$\tan \alpha = 7m/5n. \qquad (2)$$

The expressions (1) and (2) can be rewritten as

$$\begin{aligned} (5q - 1)n + (7q - 1)m &= 0 \qquad (3) \\ 5(\tan \alpha)\, n - 7m &= 0. \end{aligned}$$

The condition under which the homogeneous system (3) has a nontrivial solution for n and m is

$$\begin{bmatrix} 5q - 1 & 7q - 1 \\ 5 \tan \alpha & -7 \end{bmatrix} = 0;$$

i.e.,

$$\tan \alpha = -[7(5q - 1)/5(7q - 1)]. \qquad (4)$$

Or in general for l and s lamellae:

$$\tan \alpha = -[l(qs - 1)/s(lq - 1)]. \qquad (5)$$

Given the two thicknesses l and s of the lamellae to be mixed and given the measured q-value, the algorithm of Fig. 11 gives the desired sequence.

The relative abundances of the two kinds of tilings are given by

$$m/n = (s/l) \tan \alpha = -(qs - 1)/(lq - 1). \quad (6)$$

The width of the slit is given by

$$D = (l + s \tan \alpha)/(1 + \tan^2 \alpha)^{1/2}. \quad (7)$$

The inverse $2/D$ is a measure for the width in reciprocal space of the central peak of the Fourier transform.

Acknowledgments

The authors thank Professor J. Stoemenos, Mrs. M. Stoemenos, and Mr. C. Chrysafis for providing some of the samples.

References

1. R. F. Brebrick, *in* "The Chemistry of Extended Defects in Non-Metallic Solids" (L. Eyring and M. O'Keeffe, Eds.), p. 183, Elsevier, Amsterdam/New York (1970).
2. T. B. Zhukova and A. I. Zaslavskii, *Sov. Phys. Crystallogr.* **16,** 796 (1972).
3. I. I. Petrov and R. M. Imamov, *Sov. Phys. Crystallogr.* **14,** 593 (1970).
4. A. G. Talybov, *Sov. Phys. Crystallogr.* **6,** 40 (1961).
5. K. A. Agaev, A. G. Talybov, and S. A. Semiletov, *Sov. Phys. Crystallogr.* **13,** 44 (1968).
6. K. A. Agaev and S. A. Semiletov, *Sov. Phys. Crystallogr.* **10,** 86 (1965).
7. K. A. Agaev and A. G. Talybov, *Sov. Phys. Crystallogr.* **11,** 400 (1966).
8. I. I. Petrov, R. M. Imamov, and Z. G. Pinsker, *Sov. Phys. Crystallogr.* **13,** 339 (1968).
9. R. M. Imamov, S. A. Semiletov, and Z. G. Pinsker, *Sov. Phys. Crystallogr.* **15,** 239 (1970).
10. N. Frangis, S. Kuypers, C. Manolikas, J. Van Landuyt, and S. Amelinckx, *Solid State Commun.* **69,** 8 (1989).
11. M. Predota, L. Benes, and J. Horak, *Phys. Status Solidi A* **100,** 401 (1987).
12. W. Kullmann, J. Geurts, W. Richter, N. Lehner, H. Rauh, U. Steigenberger, G. Eichorn, and R. Geick, *Phys. Status Solidi A* **125,** 131 (1984).
13. M. H. Francombe, *Brit. J. Appl. Phys.* **9,** 415 (1958).
14. R. W. G. Wyckoff (Ed.), "Crystal Structures," Vol. 1, p. 86, Wiley–Interscience, New York (1965).
15. J. Van Landuyt, R. De Ridder, R. Gevers, and S. Amelinckx, *Mater. Res. Bull.* **5,** 353 (1970).
16. D. Van Dyck, G. Van Tendeloo, and S. Amelinckx, *Ultramicroscopy* **10,** 263 (1982).
17. K. Fujiwara, *J. Phys. Soc. Japan* **12,** 7 (1957).
18. A. Katz and M. Duneau, *J. Phys.* **47,** 181 (1986).
19. V. Elser, *Acta Crystallogr. A* **42,** 36 (1986).
20. R. K. P. Zia and W. J. Dallas, *J. Phys. A* **18,** L341 (1985).
21. D. Van Dyck *et al.*, to be published.
22. W. Coene, D. Van Dyck, J. Van Landuyt, and S. Amelinckx, *Philos. Mag. B* **56,** 415 (1987).
23. W. Coene and D. Van Dyck, *Ultramicroscopy* **15,** 41 (1984).
24. M. Van Sande, R. De Ridder, J. Van Landuyt, and S. Amelinckx, *Phys. Status Solidi A* **50,** 587 (1978).
25. G. Van Tendeloo, C. Van Heurck, and S. Amelinckx, *Solid State Commun.* **71,** 705 (1989).